Chaos, Solitons and Fractals 193 (2025) 116103

Contents lists available at ScienceDirect

Chaos, Solitons and Fractals

journal homepage: www.elsevier.com/locate/chaos

Advancing vulnerability assessment in critical infrastructure systems through higher-order cycles and community structures

Bitao Dai, Min Wu, Longyun Wang, Jianhong Mou, Chaojun Zhang, Shuhui Guo, Suoyi Tan, Xin Lu *

College of Systems Engineering, National University of Defense Technology, Changsha 410073, China

ARTICLE INFO

Keywords:
Network robustness
Network disintegration
Critical infrastructures
Community structure
Higher-order cycle
Complex network
Reliability analysis

ABSTRACT

Ensuring the stability of Critical Infrastructure Systems (CIS) is paramount for modern societies. Represented as complex networks, these systems require robust disintegration strategies to identify critical vulnerabilities and prevent systemic failures. However, existing algorithms often oversimplify interactions, assume rarely observed fully connected higher-order structures, and overlook strong community formations and indirect connections. To overcome these limitations, this study develops the Higher-Order Cycle Disintegration Framework, leveraging higher-order cycles and community structures to capture both direct and indirect interactions. Extensive experiments on synthetic and empirical networks confirm that the strategy developed within the framework dramatically outperforms existing state-of-the-art algorithms, particularly demonstrating superior early-stage disintegration capability. Specifically, it achieves improvements of up to 63.41 % and 23.83 % in R and f_c respectively, with average of 40.16 % and 16.87 % across 12 empirical networks. Unlike conventional methods, which often display a rich-club effect with tightly clustered critical nodes, our algorithm identifies a more dispersed distribution of vulnerabilities. Furthermore, Kendall's Tau analysis reveals consistently low correlations (below 0.52) with baselines, underscoring the distinctiveness and enhanced discriminative capability of our framework. These findings provide valuable insights into vulnerability assessment and the development of targeted protection strategies, advancing the long-term reliability and robustness of CIS.

1. Introduction

Assessing the robustness of Critical Infrastructures Systems (CIS) remains a complex, and evolving challenge, as these systems encompassing power grids, energy distribution, transportation, and water supply, form the backbone of modern society [1–5]. Their uninterrupted operation is imperative for ensuring socio-economic stability at regional and national levels. Nevertheless, numerous catastrophic events have exposed their vulnerabilities to disruptions, such as cyberattacks, natural disasters, and industrial accidents. For instance, the 2019 Venezuelan blackout, attributed to technical failures and cyberattacks, left millions without power, incurring losses exceeding $1 billion [6,7], while the 2021 Suez Canal blockage delayed $92.7 billion in global trade, resulting in overall economic loss of $136.9 billion [8].

The growing reliance on CIS, coupled with the evolving risk landscape, underscores the necessity for proactive robustness assessments to identify vulnerabilities and mitigate potential threats [9,10]. Robustness of CIS refers to the system's ability to maintain operational functionality and topological connectivity amidst disturbances [11,12]. Early research primarily concentrated on designing optimally robust networks or enhancing robustness through adding redundant connections or adjusting network structure [9,13–16]. However, such approaches often proved impractical, as CIS are precisely engineered for specific functions, rendering them expensive and incompatible with real-world constraints. Given these inherent structural limitations, a more practical strategy involves simulating high-impact disruptions to pinpoint vulnerabilities and implement targeted protection, essential for preventing rapid system collapse [17].

Recent advancements in complex network modeling have provided deeper insights into CIS vulnerabilities across various domains, including road networks, power grids, and communication networks [14,18]. Network disintegration, or dismantling, has proven effective in evaluating robustness by identifying critical nodes or connections whose failure could trigger systemic collapse [12,19–23]. For instance, Lordan

* Corresponding author.
E-mail address: xin.lu.lab@outlook.com (X. Lu).

https://doi.org/10.1016/j.chaos.2025.116103
Received 8 January 2025; Accepted 3 February 2025
Available online 12 February 2025

et al. assessed air transportation robustness using Bonacich power centrality [24], revealing that isolated nodes could lead to network collapse, while Ouyang et al. proposed optimization strategies for CIS protection [6]. Similarly, Wandelt et al. modeled air transportation systems as complex networks, uncovering hidden vulnerabilities and optimizing attack strategies through betweenness centrality [25,26].

Despite significant advances, optimal network disintegration strategies remain NP-hard [20], prompting the development of various heuristic approaches to facilitate disruptive attacks. Currently, network disintegration strategies are typically classified into five categories: mathematical programming models [27,28], centrality-based algorithms [1,29–31], heuristic algorithms [20,21,32,33], evolutionary algorithms [34,35], and machine learning algorithms [36,37].

Mathematical programming models, although precise, suffer from high computational complexity and are limited to specific, solvable objective functions. In contrast, heuristic and evolutionary algorithms, while offering reasonable performance, face scalability issues when applied to large networks. Recent advances in deep learning have spurred promising alternatives, with Fan et al. developing a deep reinforcement learning-based strategy and Grassia et al. employing graph neural networks for network disintegration [36,37]. Both approaches leverage geometric deep learning to develop attack strategies on small synthetic networks. These machine learning algorithms, while excelling in computational efficiency and adaptability, often trade off interpretability—a critical aspect in practical implementations.

Among these, centrality-based algorithms have gained prominence due to their interpretability and scalability, especially in CIS, where understanding structural dynamics is essential. Among them, Collective Influence (CI) and Domirank are regarded as state-of-the-art (SOTA) algorithms [30,38]. CI assesses a node's influence within a defined radius but neglects higher-order interactions and structural heterogeneity. Domirank emphasizes hierarchical dominance and rich-club structures, excelling in clustered networks but falling short in addressing dispersed vulnerabilities. These limitations highlight the need for more comprehensive models that account for indirect connections and higher-order interactions to capture the complex dynamics of CIS.

Community structures, which are prevalent in real-world networks, play a pivotal role in influencing network robustness. In particular, CIS exhibit exceptionally strong community formations due to geographic and operational constraints, further shaping their structural properties. Leveraging community structures has proven to enhance disintegration strategies significantly [14,16,39–43]. For instance, Requião et al. developed a module-based attack algorithm leveraging community structures within the US airport network [44], while Cong et al. employed spectral clustering to identify critical nodes in China's airport network [45]. These studies underscore the strong correlation between robustness and community structure, inspiring further exploration of community-based strategies for more effective disintegration.

Building on community-based strategies, higher-order structures, such as simplicial complexes, have gained attention for capturing multi-node interactions and revealing dynamics beyond pairwise relationships [46–49]. Nevertheless, traditional simplicial complex models assume fully connected higher-order structures, which are rarely present in CIS. By contrast, higher-order cycles extend these models by accommodating partially connected structures, effectively capturing both direct and indirect interactions. This flexibility enhances robustness by introducing redundant paths and dynamic feedback mechanisms, as demonstrated in studies on synchronization, connectivity, and information dissemination. For instance, Shi et al. demonstrated the significant impact of higher-order cycles on network synchronization [50–52], while Fan et al. emphasized their roles in enhancing connectivity, synchronization, and information dissemination [53,54]. In computational neuroscience, higher-order cycles facilitate neural loops, promoting feedback and information flow. Additionally, Zhao et al. proposed higher-order centralities based on higher-order cycles, demonstrating superior performance in synchronization and virus containment [55]. Despite the potential of higher-order cycles, existing algorithms have yet to fully exploit this advantage, especially within CIS contexts.

Building on these insights, current network disintegration strategies based on classical centrality metrics and community-based approaches, fail to capture the complex, multi-dimensional interactions in CIS. Traditional higher-order models, assume fully connected higher-order structures, which are rarely present in CIS due to their operational and geographic constraints. This limitation hampers the ability to model the partial connectivity and indirect interactions that are crucial to accurately assessing network vulnerabilities. To address these gaps, this study introduces the Higher-Order Cycle Disintegration Framework, which integrates higher-order cycles and community structures to provide a more precise and dynamic model of CIS vulnerabilities. By incorporating both direct and indirect network interactions, the introduced algorithm under the framework significantly advances existing algorithms, enhancing the accuracy of vulnerability detection and optimizing resilience strategies against both natural and man-made disruptions.

The rest of this paper is structured as follows. Section 2 outlines the fundamental definitions and theories related to simplicial complexes and higher-order cycle. Section 3 discusses the of Higher-Order Cycle Framework, along with the synthetic and empirical network datasets used in the analysis. Section 4 presents disintegration results for synthetic and empirical networks, offering a systematic exploration of the underlying mechanisms. Finally, Section 5 summarizes the key findings of the research and suggests potential directions for future investigation.

2. Preliminaries

2.1. Graph theory

In Graph theory, networks are conceptualized as assemblies of nodes, representing distinct entities interconnected by edges to delineate their relationships. A graph $G = (V, E)$ is defined as an undirected network composed of $N = |V|$ nodes and $M = |E|$ edges, where $V = \{v_1, v_2, \cdots, v_N\}$ represents the nodes set, and $E \subseteq V \times V = \{(u, v)|u, v \in V\}$ represents the edges set between nodes pairs. The adjacency matrix $A(G) = (a_{ij})_{N\times N}$ characterizes the network, where $a_{ij} = 1$, if v_i and v_j are directed connected, and $a_{ij} = 0$ otherwise. The topological properties of network can be further explored by detecting community structures, denoted as $\{c_1, c_2, \cdots c_k\}$ employing certain community detection algorithm.

When a node is removed from the network, all its attached edges are also removed from the network. Let vector $\widehat{n} = [n_1, n_2, \cdots n_N]$ represent the status of nodes, where $n_i = 0$ indicates v_i is removed and $n_i = 1$ otherwise. The fraction of removed node is expressed as $q = 1 - \frac{\sum_i n_i}{N}$, resulting in the emergence of a residual network $\widehat{G} = (V\backslash\widehat{V}, E\backslash\widehat{E})$ with $\widehat{V} \subseteq V$ and $\widehat{E} \subseteq E$ representing the set of targeted removed nodes and edges.

2.2. Network disintegration

The functionality of a network is intrinsically linked to its connectivity, which determines the operation of networked systems. The extent of network damage upon node removal is quantified by $S(q)$ reflecting the size of the largest connected components remaining. Network disintegration can be formulated as identifying a minimal node set $\widehat{V}$ that maximizes the attack effect. In this study, we explore the efficiency of network disintegration strategies through the critical removal fraction f_c and the Schneider R [56].

The critical removal fraction f_c represents the minimum proportion of nodes required to induce network collapse, where $S(q) \leq \sigma$. It is determined by calculating the number of nodes N_r that must be removed until $S(q) < \sqrt{N}$, indicating near-total disconnection and severe impairment of network functionality:

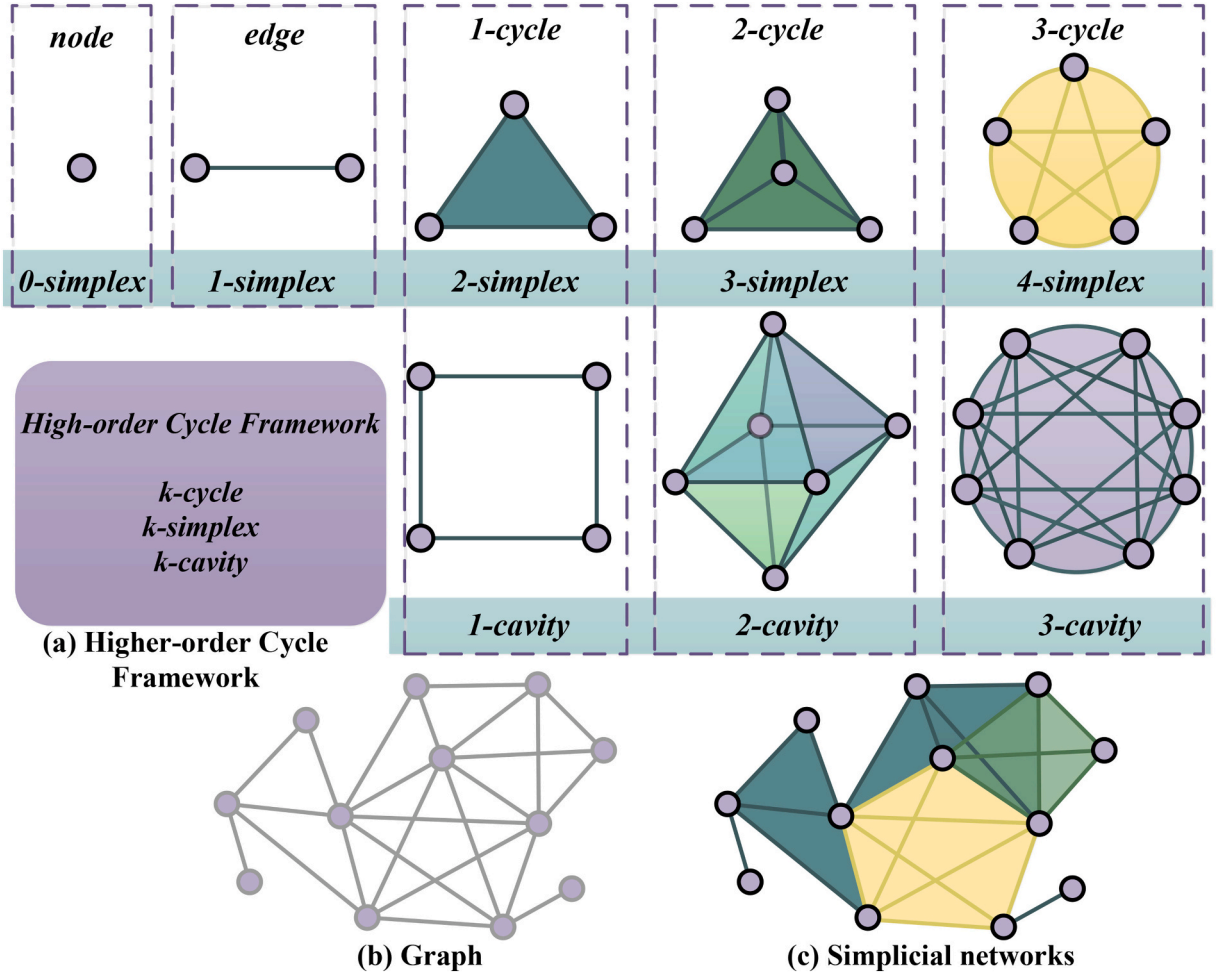

Fig. 1. Higher-order representations. (a) Illustrating the Higher-Order cycle framework. (b) and (c) Demonstrating the simplicial networks.

$$f_c = \frac{N_r}{N} \tag{1}$$

Concentrating solely on f_c may overlook scenarios where substantial damage does not culminate to complete network failure. To address this, we introduce the Schneider R which assesses the network robustness based on its response to various levels of attack intensity:

$$R = \frac{1}{N}\sum_{Q=1}^{N} s(Q) \tag{2}$$

where $s(Q) = S(Q)/N$ and the value of Schneider R spans from 0, indicative of networks with isolated nodes, to 0.5 for highly robust, fully interconnected networks.

Consequently, network disintegration could be modeled as an optimization problem aimed at minimizing either the critical removal fraction f_c or Schneider R:

$$\begin{aligned} &Minimize f_c \text{ or } R \\ &s.t. \begin{cases} Q = N - \sum_{i=1}^{N} n_i \\ n_i \in \{0,1\}, \quad (i = 1,2,\ldots,N) \end{cases} \end{aligned} \tag{3}$$

In addition, we employ the promotion ratio to effectively assess the algorithm's performance. This metric measures the relative improvement of our algorithm over existing baselines and are defined by:

$$\begin{aligned} \varphi^{f_c} &= \frac{\left(f_c^{optimal}baseline - f_{c\ our\ algorithm}\right)}{f_c^{optimal}baseline} \times 100\% \\ \varphi^{R} &= \frac{\left(R^{optimal}{}_{baseline} - R_{our\ algorithm}\right)}{R^{optimal}{}_{baseline}} \times 100\% \end{aligned} \tag{4}$$

2.3. Higher-order representations

Given that CIS exhibit strong community structures and rarely feature fully connected higher-order structures, we use higher-order cycles to capture both the direct and indirect complex interdependencies within these systems.

Simplices and simplicial complexes are key components of higher-order cycles, providing an extended framework that goes beyond pairwise interactions to incorporate linearly (in)dependent cycles and cavities (as shown in Fig. 1 and further elaborated in Supplementary note 1). Higher-order cycles reveal the intricate connectivity patterns within networks, capturing both direct interactions between nodes and the subtle influences arising from non-adjacent, indirect connections. Simplicial complexes are particularly advantageous because they represent both higher-order interactions and encompass traditional pairwise interactions. This versatility makes them an effective tool for capturing the complex interplay of both dense and sparse relationships in networked systems bridging the gap between geometric structures and network topological properties.

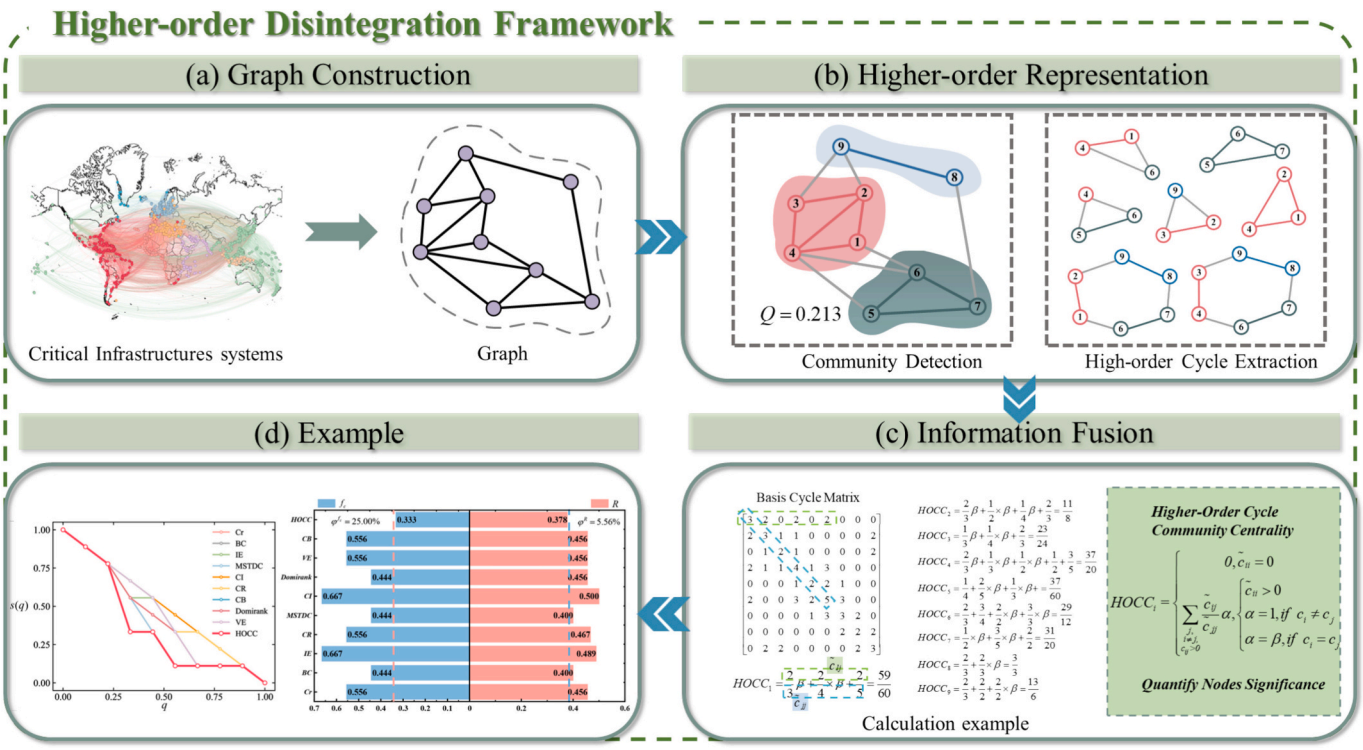

Fig. 2. Higher-order disintegration framework.

Definition 1. (*Simplex*) In the context of algebraic geometry, a simplex is a fully connected sub-network, commonly known in graph theory as a clique. Specifically, a $k-simplex$ α_k consisting of $k+1$ vertices $\{v_1, v_2 \cdots, v_{k+1}\}$, where every possible subset of these vertices constitutes a face of the simplex. As demonstrated in Fig. 1, a node is a $0-simplex$, an edge is a $1-simplex$, a triangle is a $2-simplex$ and a tetrahedron is a $3-simplex$.

Definition 2. (*Faces of a Simplex*) A face of a simplex is any lower-dimensional simplex formed by a subset of the vertices of the original simplex. Specifically, for a $k-simplex$ α_k, any $j-simplex$ $(0 \le j \le k)$ formed by its vertices is considered a face of α_k. For instance, as illustrated in Fig. 1, the faces of a 3-simplex include four 0-simplex, six $1-simplex$, four $2-simplex$ and one $3-simplex$.

Definition 3. (*Simplicial Complexes*) A simplicial complex $K = [\alpha_0, \alpha_1, \ldots, \alpha_k]$ is a collection of simplices that satisfies closure and intersection conditions.

1. **Closure Condition**. If a simplex belongs to a simplicial complex, then all faces of must also be included too.
2. **Intersection Condition**: The intersection of any two simplices in K is either empty or itself a simplex. This means that every face of a simplex in the complex is also in the complex, and the intersection of any two simplices is either empty or a common face of both.

Based on these definitions, networks can be conceptualized as simplicial networks, where each node represents a simplex (as illustrated in Fig. 1(a)). This representation captures both pairwise interactions and complex interplay among multiple nodes.

According to [50,51], simplices and simplicial complexes serve as fundamental components of higher-order cycles, capturing both linear (in)dependencies and cavities (see Fig. 1(c). and Supplementary note 1). Higher-order cycles reveal intricate connectivity patterns within networks, encompassing direct edges and subtle indirect influences. The smallest unit of a cycle is a triangle, i.e., $2-simplex$, which corresponds to $1-cycle$ in the higher-order cycle framework. Extending this concept, a $3-simplex$, represents a $2-cycle$, while a $4-simplex$ represents a $3-cycle$ and so forth.

Given the structural characteristics of CIS, fully connected multi-node interactions are rarely observed, while indirect connections are more universal. Therefore, we leverage basic cycle, known as cycle basis, defined as the minimal ensemble of cycles capable of generating all conceivable cycles within a graph through linear combinations as the foundation of the graph's cyclic topology. This structural information is used to design an effective disintegration algorithm, as detailed in Supplementary note 2. By combining the strengths of higher-order cycles, our framework captures both higher-order interactions and real-world structural properties of CIS, enabling practical and effective solutions for network disintegration.

3. Data and method

3.1. Higher-order disintegration framework

As depicted in Fig. 2, the core of proposed Higher-Order Disintegration Framework primarily comprises higher-order representations and information fusion. Building upon this framework, the introduced Higher-Order Cycle Community Centrality (*HOCC*) algorithm incorporates three critical components: community structure, higher-order cycles, and their collective integration.

Initially, we identify the basis cycle to capture the high-order cycle information. Let S_i denote the set of basic cycles associated with v_i, and $S = \cup_{v_i \in V} S_i$ represent the set of all basic cycle in G. The cycles in-

Table 1
The centralities of nodes across different algorithms in toy network.

Node	Cr	BC	IE	CR	MSTDC	CI	Domirank	VE	CB	HOCC
1	0.65	0.04	1.09	2.17	12.00	16.00	−3.15	−0.09	3.00	1.97
2	1.26	0.13	1.36	4.00	20.00	18.00	5.85	−0.28	3.00	2.08
3	0.65	0.05	1.08	2.92	12.00	16.00	−2.89	−0.11	2.00	1.25
4	1.99	0.24	1.60	4.33	23.00	16.00	7.21	−0.38	4.00	3.70
5	0.65	0.05	1.08	2.92	11.00	16.00	−3.15	−0.11	2.00	1.23
6	1.26	0.13	1.36	4.00	18.00	18.00	5.85	−0.28	5.00	4.83
7	1.39	0.13	1.06	1.83	18.00	16.00	0.68	−0.30	3.00	2.10
8	2.00	0.08	0.69	0.00	12.00	10.00	−4.25	−0.06	2.00	2.00
9	1.39	0.13	1.06	1.83	16.00	16.00	−2.89	−0.30	3.00	4.33

teractions are encapsulated by the basic cycle matrix $\widetilde{C} = [\widetilde{c}_{ij}]_{N\times N}$, which quantifies the shared basic cycles between v_i and v_j ($i \neq j$). The element $\widetilde{c}_{ij}$ indicates the number of cycles in S that pass through v_i and v_j. For $\widetilde{c}_{ij} > 0$, v_i and v_j must be not only be part of the same cycle but also be directly connected, i.e., $a_{ij} = 1$, while the diagonal element $\widetilde{c}_{ii}$ represents the number of cycles involving v_i. Interactions between nodes lacking direct links are excluded, as our experiments reveal that considering such non-adjacent interactions neither enhances efficiency nor contributes to overall effectiveness and may even have negative impacts. This underscores the significance of direct neighborhood interactions in network robustness. For illustration, although v_6 and v_9 participate in 2 basic cycles ($\{1,2,9,8,7,6\},\{4,3,9,8,7,6\}$) as shown in Fig. 2(b), their lack of direct connection results in $\widetilde{c}_{69} = 0$, since $a_{69} = 0$, whereas v_1 and v_4 ($\{1,4,6\},\{1,2,4\}$), which also share two basic cycles and are directly connected, yield $\widetilde{c}_{14} = 2$, due to $a_{14} = 1$.

Meanwhile, we also record the values of Basic Cycle (the number of nodes participate in S, i.e., the length of S_i) of v_i which equal to $\widetilde{c}_{ii}$ as part of an ablation study to examine the impact of excluding neighborhood interactions on disintegration performance.

Beyond cycle-based interactions, it is equally essential to incorporate community-level information, particularly accounting for the influence of edges spanning across different communities. Nodes within the same community frequently share neighbors and exert overlapping influence, necessitating careful consideration of their intertwined effects. To effectively capture these relationships, we employ the Louvain algorithm [57] to partition the network G into community structures $C = \{c_1, c_2, \cdots c_k\}$. Subsequently, to achieve a unified representation, we fuse the information from both higher-order cycles and community structures, leading to the development of the Higher-Order Cycle Community Centrality (*HOCC*):

$$HOCC_i = \begin{cases} 0, & \widetilde{c}_{ii} = 0 \\ \sum\limits_{\substack{j, \\ i\neq j, \\ c_{ij}>0}} \frac{\widetilde{c}_{ij}}{\widetilde{c}_{jj}}\alpha, & \begin{cases} \widetilde{c}_{ii} > 0 \\ \alpha = 1, if\ c_i \neq c_j \\ \alpha = \beta, if\ c_i = c_j \end{cases} \end{cases} \tag{5}$$

in which α captures the impact of edges spanning across communities, while c_i indicates the community affiliation of v_i. The parameter β ($0 \leq \beta \leq 1$) serves as a penalty coefficient, strategically applied to account for the structural heterogeneity both within and between communities. To identify the optimal β, we conduct a grid search with a step size of 0.02.

The ratio $\frac{\widetilde{c}_{ij}}{\widetilde{c}_{jj}}$ evaluates a node's significance subject to its involvement in shared basis cycle relative to its neighbors. Specifically, the numerator captures the number of shared cycles associated with node and its neighbor, while the denominator represents the total number of cycles involving the neighbor. This formulation provides a nuanced perspective on a node's centrality by accounting for both its individual cycle participation and the complex interplay between network cycles and community structures.

To further illustrate the proposed Higher-Order Disintegration Framework and the introduced *HOCC* algorithm, we introduce a toy network with a modularity of 0.213, indicating a relatively weak community structure, as depicted in Fig. 2(b). Initially, we extract the basis cycles of the network, denoted by S, with size of 7, and subsequently calculate each node's *HOCC* value according to Eq. (1), with the detailed calculation process shown in Fig. 2(c).

Table 1 presents the centrality values of nodes derived from various baselines (see Section 3.4 for details), highlighting significant discrepancies in the rankings across different algorithms. We further assess the effectiveness of each algorithm in terms of network disintegration, with the outcomes illustrated in Fig. 2(d). It can be observed that the f_c and R associated with the *HOCC* algorithm yield optimal results, as indicated by a disintegration curve that consistently lies at the lowest tier, demonstrating superior disintegration efficacy.

The results unequivocally demonstrate that the *HOCC* algorithm integrates both higher-order cycle and community structure information, providing a comprehensive understanding of network robustness. This integration not only captures the complexity of network interactions but also ensures that the disintegration strategy is both targeted and efficient. In the following sections, we will delve deeper into evaluating the performance of our algorithm, utilizing both synthetic and real-world networks to further substantiate its effectiveness in network disintegration strategies.

3.2. Complexity analysis

The overall complexity of *HOCC* is primarily driven by the community detection algorithm, the cycle basis search algorithm and the nested loops that compute the shared cycles between pairs of neighbors. The complexity of the community detection algorithm varies from practical reality. For instance, Louvain algorithm has a complexity of $O(MlogN)$. As discussed in Supplementary note 2, the complexity of cycle basis search algorithm is $O(M+N)$. Regarding nested loops, initializing all nodes in V takes $O(N)$, and for each node, iterating over its neighbors involves a worst-case complexity of $O(|\Delta|)$, where Δ is the maximum degree of the graph and is dramatically smaller than N. Therefore, the overall computational complexity of *HOCC* is $O(MlogN) + O(M+N) + O(N{\cdot}\Delta) \approx O(N)$, enabling it sufficiently adaptable for large-scale networks. The space complexity is $O(|N|)$, accounting for the storage of *HOCC* scores, the cycle basis set and temporary neighbor set. This en-

Table 2
Basic statistics of empirical networks.

Networks	*N*	*M*	*Diameter*	$\langle k \rangle$	*C*	$\bar{l}$	*D*
Sydney	32,956	38,787	239	2.35	0.01	77.28	0.0001
Chicago	12,979	20,627	106	3.18	0.04	41.97	0.0002
Birmingham	14,578	20,913	135	2.869	0.148	41.719	0.0002
Power	5,300	8,271	49	3.12	0.09	20.85	0.0006
Europe	13,478	16,922	147	2.511	0.089	49.505	0.0002
Goldcoast	4,783	5,952	127	2.489	0.042	50.371	0.0005
Fiber	154	206	21	2.68	0.08	8.46	0.0175
Grid	4,941	6,594	46	2.67	0.08	18.99	0.0005
Sketch	933	1,475	32	3.16	0.03	12.68	0.0034
North	14,990	18,804	138	2.509	0.084	47.504	0.0002
London	488	729	33	2.99	0.02	13.84	0.0061
Chilean	347	444	23	2.559	0.087	8.155	0.0074

sures that the method is efficient in terms of memory usage.

Algorithm 1. *HOCC* calculation.

Input: Graph $G=(V,E)$, penalty coefficient β, community detection algorithm.
Output: Ranking node list.

Initialize an empty dictionary dic with keys as node IDs and values set to zero: $dic \leftarrow \{0 | v_i \in V\}$.
Execute specific community detection algorithm to obtain node communities: $C \leftarrow \{c_i | v_i \in V\}$.
Execute the cycle basis search algorithm to obtain the basic cycle set S_i associated with v_i, and the all basic cycle set $S=\cup_{v_i \in V} S_i$ in G.
For each node $v_i \in V$ do:
  $\tau_i \leftarrow$ Set of neighbors of v_i.
  For each neighbor $v_j \in \tau_i$ do:
    If v_i and v_j in S_i then:
      $\lambda_{jj} \leftarrow$ the number of shared cycles in S_j.
      $\lambda_{ij} \leftarrow$ the number of shared cycles in S_i that pass through v_i and v_j.
    If $c_i = c_j$ then:
      $\theta = \lambda_{ij} / \lambda_{jj} * \beta$.
    Else:
      $\theta = \lambda_{ij} / \lambda_{jj}$.
    $dic[i] = dic[i] + \theta$.
  End for.
End for.
Ranking dic by value.
Return index list of dic.

well as parameters for minimum and maximum community size. Specifically, the adjusted parameter (μ) determines the proportion of links a node shares with nodes outside of its community, controlling the modularity of community structures. In our study, we fix certain parameters ($\mu = 0.05$, $\tau_1 = 3$, $\tau_2 = 2$, $k_{\max} = 40$), while varying network size ($N = 1000, 2000, 3000$) and average degree from 9 to 15 to investigate how changes in network density and scale influence the disintegration efficacy of the *HOCC*. The topological characteristics of the synthetic networks are summarized in Supplementary note 3.

3.3. Network data

3.3.1. Synthetic networks

To evaluate the performance of the proposed *HOCC* algorithm under controlled conditions, we utilize synthetic networks generated by the Lancichinetti–Fortunato–Radicchi (LFR) [58] model. The LFR model is specifically designed to emulate real-world networks by assuming that both the degree distribution and community size follow power-law distributions, which closely mimic the heterogeneous nature of real-world networks. This enables us to rigorously test the robustness and effectiveness of our algorithm in various network configurations.

The LFR networks are characterized by several critical parameters, including the number of nodes (N), community adjusted parameter (μ), average degree ($\langle k \rangle$), maximum degree ($k_{\max}$), minimum degree ($k_{\min}$), power-law exponents for the degree (τ_1), and community size (τ_2), as

3.3.2. Empirical networks

To capture the intricacies of real-world critical infrastructure systems, we extend our analysis to twelve real-world networks from various domains. These include public transit networks—the large-scale Chicago Urban transportation network (Chicago), the small-scale Chicago Sketch transportation network (Sketch), and the Gold Coast transportation network (Goldcoast) [59]; a communication network—the American Fiber Network (Fiber); power grid networks—the Bcspwr10 Power Grid network (Power), the American Grid (Grid), the European Grid (Europe), the Central Chilean Grid (Chilean), and the North

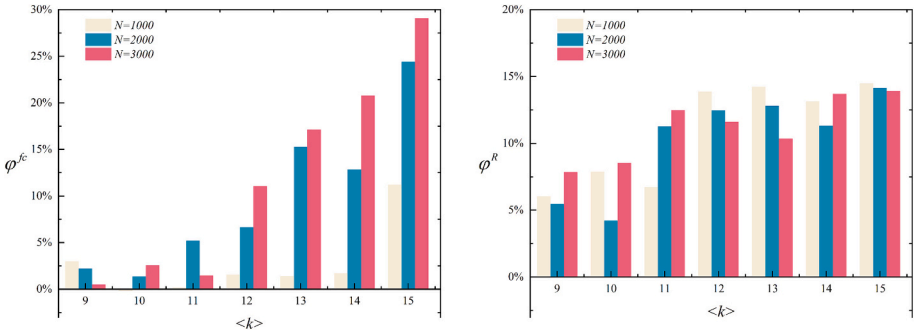

Fig. 3. Disintegration performance of *HOCC* in synthetic networks. (a) φ^{fc}. (b) φ^{R}. Each data marker corresponds to an aggregation over 300 independent realizations.

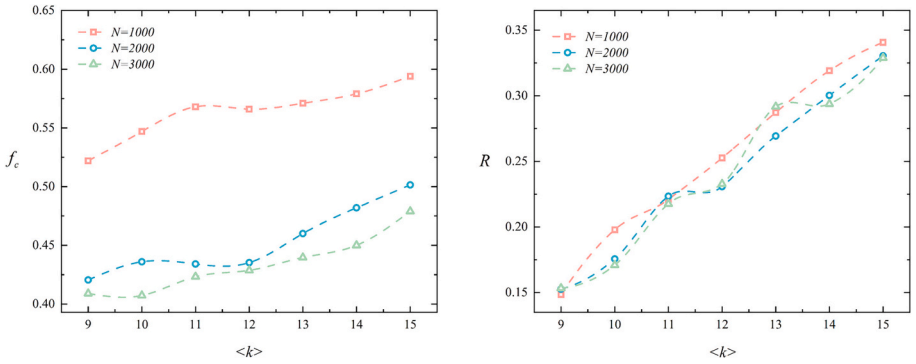

Fig. 4. Performance analysis in LFR networks. (a) f_c. (b) R. Each data marker corresponds to an aggregation over 300 independent realizations.

American Grid (North) [60,61]; and road networks—the Sydney road network (Sydney), the Birmingham road network (Birmingham), and the London road network (London) [61]. These networks are considered undirected and unweighted. We focus our analysis on the giant connected components of each network, excluding self-loops, directional attributes, and edge weights. Detailed topological summaries of these empirical networks are presented in Table 2.

3.4. Baselines

In the comparative analysis, we conduct a rigorous evaluation of various state-of-the-art (SOTA) structural-based algorithms to provide a comprehensive assessment. These include Cluster Rank (Cr) [62], Information Entropy Centrality (IE) [63], Collective Influence Centrality (CI) [38], Cycle Ratio (CR) [53], Multi-Spanning Tree-based Degree Centrality (MSTDC) [43], Betweenness Centrality (BC) [25,64], Vertex Entanglement Centrality (VE) [65], and Domirank Centrality [30]. Additionally, we conduct an ablation study by omitting community structures, referred to as Cycle Basis Centrality (CB), which represents the number of basic cycles a node participates in, for comparison. To further substantiate our evaluation, we utilize Kendall's Tau [66] to measure the correlation between the node rankings produced by our proposed algorithm and those generated by baselines. This enables us to assess whether our algorithm uncovers novel insights or captures previously overlooked structural information, offering a deeper understanding of its potential advantages.

4. Results

In this section, we provide a thorough evaluation of the performance and efficiency of *HOCC* through numerical experiments conducted on both synthetic and empirical networks. We then explore how different network structures influence the effectiveness of our algorithm in synthetic networks. To strengthen our analysis, we perform a correlation comparison between our algorithm and existing algorithms, highlighting differences in distribution. This comparison offers deeper insights into the unique advantages of our Higher-Order Cycle Disintegration Framework.

4.1. Performance in synthetic networks

For synthetic networks, we systematically analyze the impact of average degree $\langle k \rangle$ and network size N on the performance improvement of our algorithm compared to the state-of-the-art (SOTA) algorithms. As demonstrated in Fig. 3, our algorithm consistently outperforms the SOTA algorithms across all settings in terms of both the f_c and R metrics, achieving substantial enhancements under various configurations. Specifically, the proposed algorithm exhibits the most significant improvement for f_c, with a maximum enhancement of 29.07 % observed in the LFR_3000_15 network ($N = 3000$, $\langle k \rangle = 15$). Moreover, φ^{f_c} exhibit exceedingly sensitivity to the network size and average degree. For a fixed average degree (e.g., $\langle k \rangle = 15$), φ^{f_c} consistently improves as network size increases, rising from 11.21 % at $N = 1000$ to 29.07 % at $N = 3000$. Similarly, for a fixed network size (e.g., $N = 2000$), φ^{f_c} profoundly increases from 2.21 % to 24.42 % as the average degree increases. These trends highlight the algorithm's ability to effectively leverage higher-connectivity conditions, particularly in larger networks with higher average degrees.

In terms of R, the performance improvement ranges from 4.23 % to 14.49 %, with the highest improvement observed in the LFR_1000_15 network. A notable trend is the substantial improvement in improvement as the average increases. For a fixed network size (e.g., $N = 3000$), φ^{R} profoundly increases from 7.84 % to 13.90 % as the average degree increases, Emphasizing the algorithm's adaptability to denser connectivity structures. Unlike f_c, φ^{R} exhibit relative less sensitivity to network size, for a fixed average degree, the R improvement remains relatively

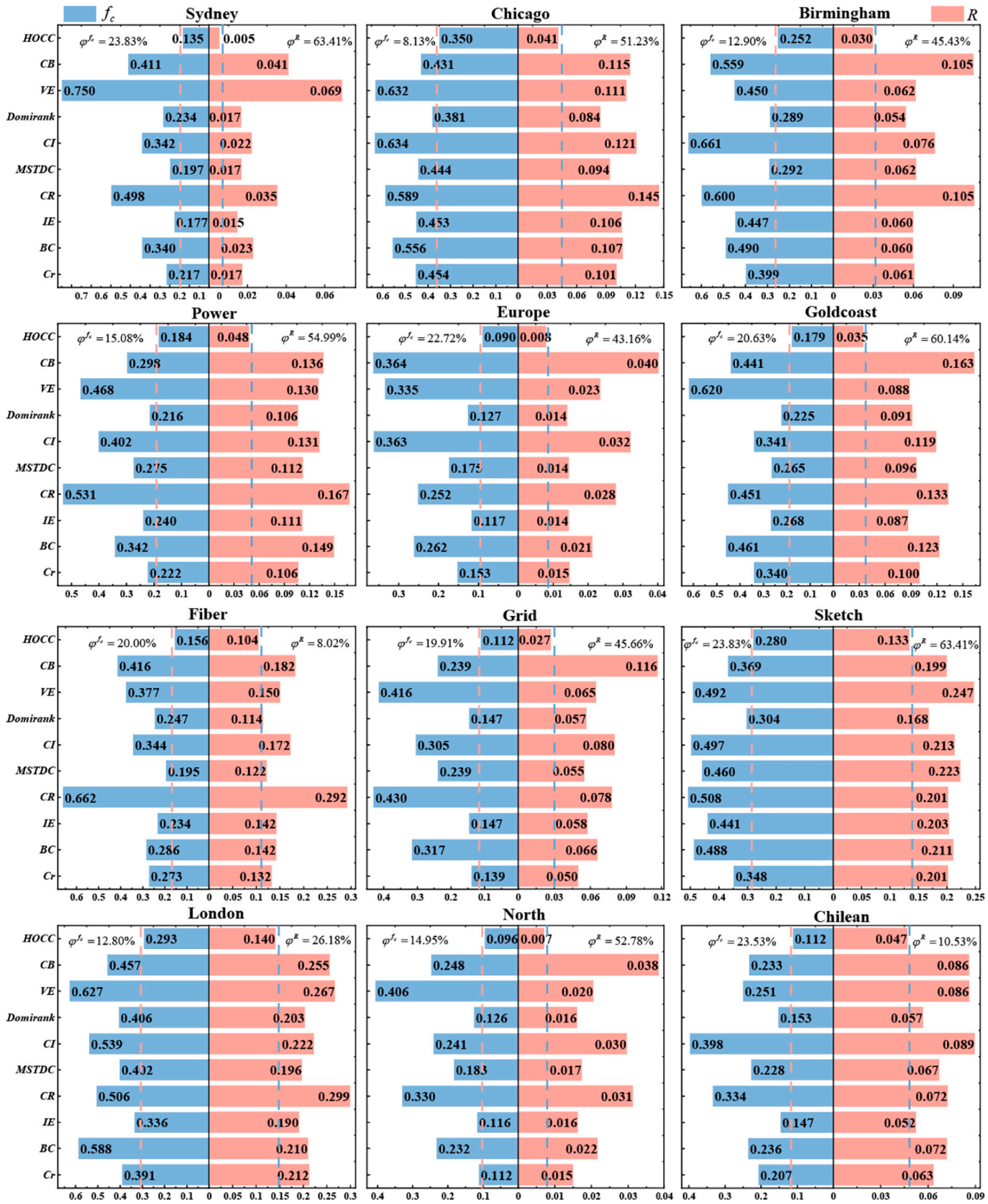

Fig. 5. Comparison of disintegration strategies on empirical networks. The blue bars indicate f_c and red bars indicate R. (For interpretation of the references to color in this figure legend, the reader is referred to the web version of this article.)

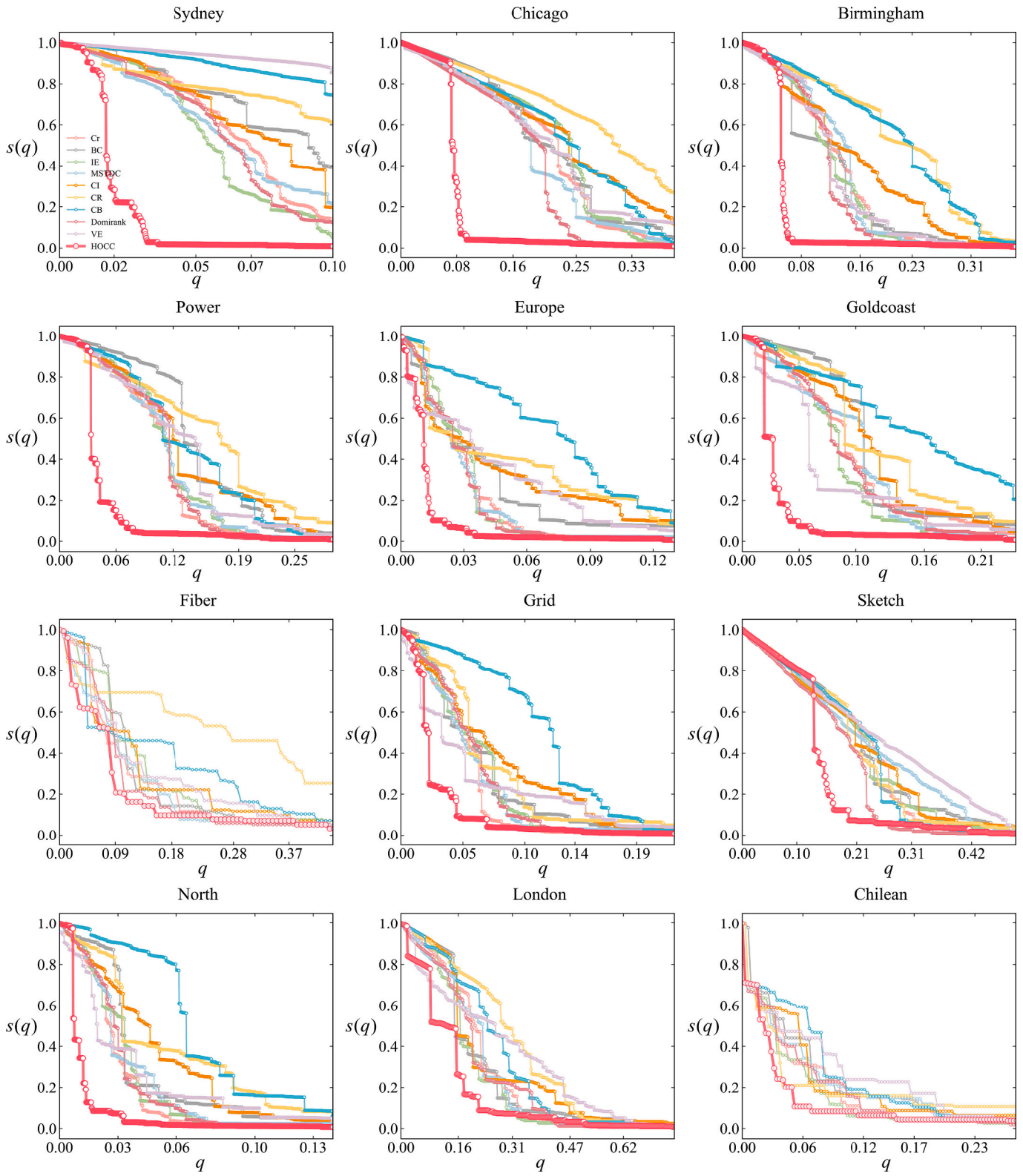

Fig. 6. Comparison of disintegration strategies on empirical networks. q indicates the proportion of removed nodes.

consistent across different network sizes.

Both metrics demonstrate that higher $\langle k \rangle$ contribute to greater performance improvement, underscoring the algorithm's capacity to exploit increased connectivity compared to the SOTA. Interestingly, the trends diverge with respect to network size: f_c benefits more from larger networks, while R exhibits diminished sensitivity to scale. These findings demonstrate the algorithm's robustness and scalability, particularly in networks characterized by high connectivity.

We further conduct a comprehensive analysis to investigate the effects of network size and average degree on the performance of our algorithm, as illustrated in Fig. 4. The results reveal distinct patterns in f_c and R with respect to N and $\langle k \rangle$. In terms of f_c, it demonstrates a

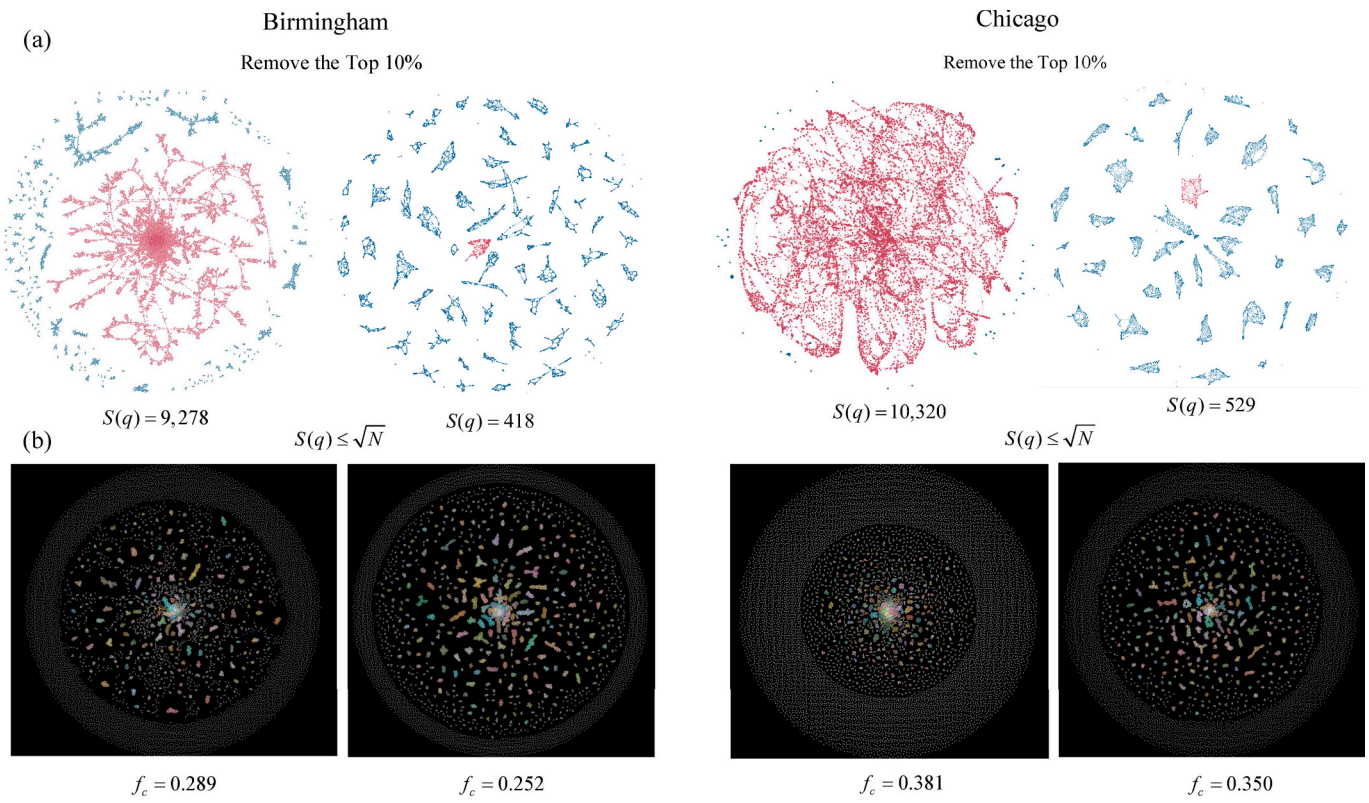

Fig. 7. Comparison of DomiRank and *HOCC* on empirical networks. In each subplot, the left image represents DomiRank, while the right represents *HOCC*. (a) Removing top 10 % of nodes. $S(q)$ below each diagram represents the size of the largest connected component for the corresponding algorithm, represented by the red subgraph. (b) Removing nodes until $S(q) \le \sqrt{N}$ the value at the bottom center of each diagram represents the f_c for the corresponding algorithm. (For interpretation of the references to color in this figure legend, the reader is referred to the web version of this article.)

consistent increase with higher $\langle k \rangle$ across all network sizes, indicating that denser networks are inherently more resistant to disintegration. For instance, when $N = 1000$, f_c increases from approximately 0.52 at $\langle k \rangle = 9$ to 0.59 at $\langle k \rangle = 15$, while for $N = 3000$, f_c increases from 0.40 to 0.48 within the same range of $\langle k \rangle$. Furthermore, f_c demonstrates marked sensitivity to network size. At a fixed $\langle k \rangle$ (e.g., $\langle k \rangle = 9$), larger networks ($N = 3000$) exhibit lower f_c (0.40) compared to smaller networks ($N = 3000$, $f_c = 0.52$). This pattern underscores the superior performance of the proposed algorithm in disintegrating large-scale networks under equivalent connectivity conditions.

Similar to f_c, R also exhibit an increasing pattern with higher $\langle k \rangle$, emphasizing the increasing difficulty of disintegration in denser networks. For instance, when $N = 1000$, R increases from 0.15 at $\langle k \rangle = 9$ to 0.34 at $\langle k \rangle = 15$. Similarly, for $N = 3000$, R increase from 0.15 to 0.33 over the same range of $\langle k \rangle$. Nonetheless, unlike f_c, R is relatively less sensitive to network size. At a fixed $\langle k \rangle$, the magnitude of divergence in R across different network sizes is less pronounced, indicating a relative insensitivity of this metric to scale.

These findings suggest that both f_c and R increase with higher $\langle k \rangle$, indicating that disintegration becomes more difficult in denser networks. Besides, f_c is more sensitive to network size, as larger networks tend to show lower f_c values at the same average degree, suggesting that our algorithm is more effective in disintegrating larger networks. In contrast, R, while still influenced by network size, shows minimal variation when compared to f_c, particularly when the average degree is held constant. This underscores its primary focus on assessing the inherent difficulty of network disintegration due to connectivity ($\langle k \rangle$), rather than being significantly affected by network scale.

4.2. Performance in empirical networks

4.2.1. Comprehensive performance

Fig. 5 presents the comparative assessment of our algorithm's performance against SOTA across twelve empirical networks with diverse structural characteristics. These results consistently demonstrate the superior performance of our algorithm in terms of both f_c and R.

In terms of f_c, the promotion rates vary from 7.95 % in Sketch network to 23.83 % in the Sydney network, with an average improvement of 16.87 % across all networks. The highest improvement in fc is observed in f_c Sydney network, which features the largest size $N = 32,956$, sparse connectivity $D = 0.0001$, and a low clustering coefficient $C = 0.07$. These structural features amplify the algorithm's ability to fragment sparse and globally connected systems. Conversely, networks with higher clustering and shorter path lengths, such as Sketch ($C = 0.03$, $\bar{l} = 12.68$) and London ($C = 0.016$, $\bar{l} = 13.84$), exhibit lower φ^{f_c}, reflecting the algorithm's relatively reduced effectiveness. This is due to the localized cohesion within these networks, where connectivity is concentrated within small, highly clustered communities. Among the SOTA algorithms, MSTDC and Domirank emerge as the most competitive alternative for f_c, achieving relatively strong results in several networks, though it still falls short of *HOCC*.

Regarding R, the promotion rates exhibit a broader range, spanning from 8.02 % in Fiber network to 63.41 % in Sydney network, with an average improvement of 40.16 % across all networks. The Sydney network's long average path length $\bar{l} = 77.28$ emphasize the algorithm's capability to disrupt large-scale with extensive global connections. Other networks, such as Goldcoast (60.14 %) and North (52.78 %)

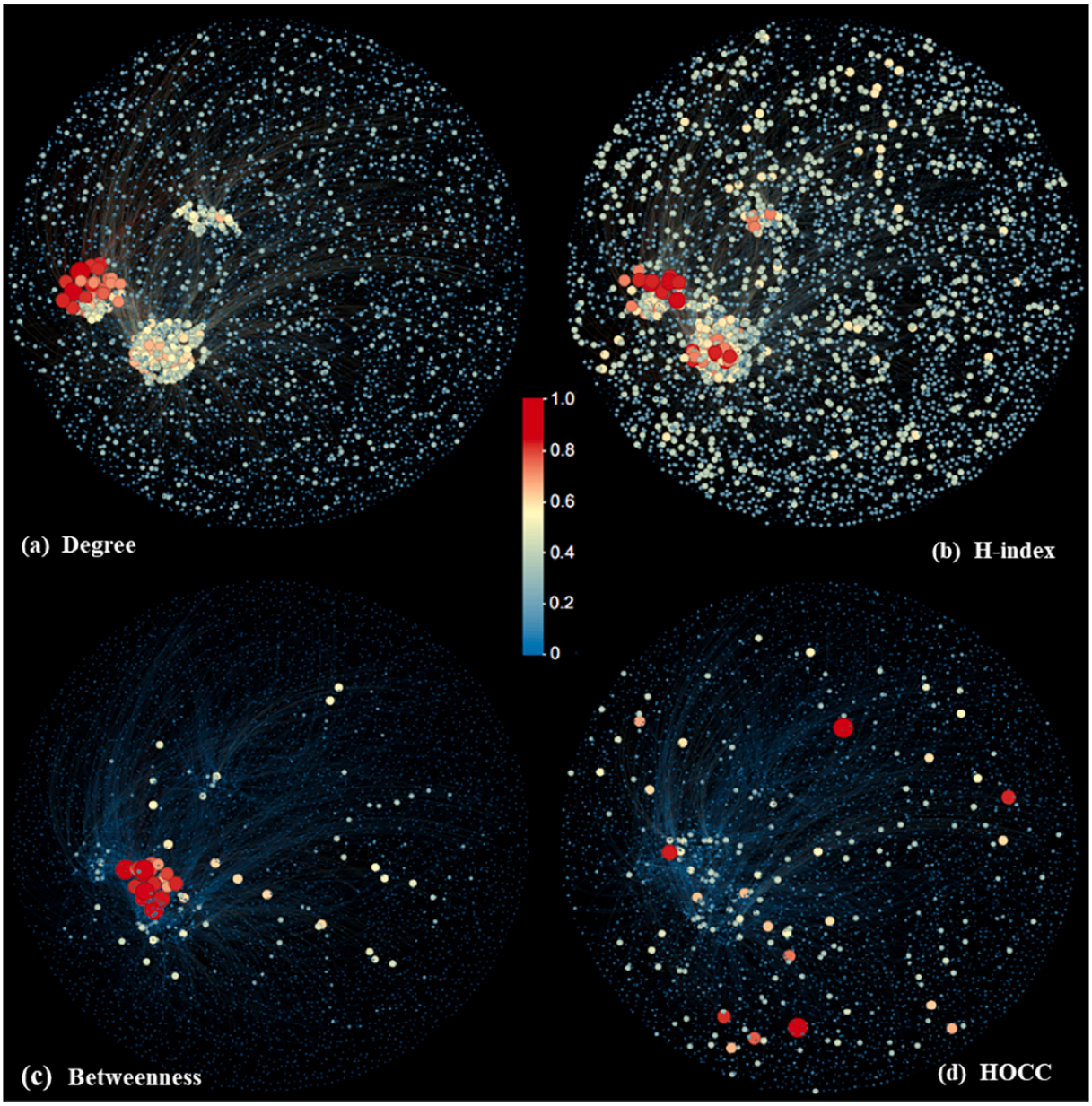

Fig. 8. Visualization of node rankings based on degree, H-index, betweenness centrality, and *HOCC* in grid network. In each plot, node sizes and colors are scaled proportionally to their respective index values, while node positions remain consistent across all plots for direct comparison.

similarly achieve high φ^R, underscoring the algorithm's efficacy in disintegrating large-scale, low-density systems. In contrast, networks like Fiber ($N = 154$, $D = 0.0175$) and Chilean ($N = 347$, $D = 0.0074$) exhibit relatively limited R improvements due to their small size and dense local connectivity, which inherently enhances structural robustness against disruption. Among the SOTA strategies, Domirank demonstrates the optimal for R in most networks.

4.2.2. Disintegration process

To further explore the disintegration process under various strategies, we analyze the relative size of the largest connected component $s(q) = S(q)/N$ as a function of the fraction of removed nodes, as illustrated in Fig. 6. Across all empirical networks, the proposed algorithm consistently outperforms other SOTA algorithms, demonstrating a more efficient disintegration process. Notably, the removal of nodes guided by *HOCC* leads to a remarkable faster collapse of network connectivity compared to SOTA.

In networks such as Sydney, Chicago, Power, and Grid, the *HOCC* algorithm exhibits exceptional efficiency, achieving a drastic reduction in $s(q)$ with the removal of <8 % of nodes. For instance, in Sydney network, the elimination of just approximately 3 % of nodes reduces $s(q)$ to below 0.01, while in Chicago network, removing 8 % of nodes brings $s(q)$ below 0.03. These results underscore the ability of *HOCC* algorithm to target critical nodes effectively. Similarly, in Power and Grid networks, the *HOCC* algorithm achieves rapid collapse with minimal node removal, further highlighting its superior performance in infrastructure networks.

In contrast, algorithms like MSTDC and Domirank show competitive disintegration results in some networks but are generally suboptimal compared to *HOCC*. For example, MSTDC performs well in the early stages of node removal across most networks but struggles to maintain its effectiveness in later phases, as observed in the Gold Coast and North networks. This suggests that while MSTDC may expedite the initial phases of disintegration, it lacks the ability to fully dismantle more robust systems.

Additionally, Cycle Basis (CB) consistently underperforms compared

Fig. 9. The correlation matrix between *HOCC* and benchmarks in empirical networks.

to *HOCC* primarily due to the omission of community structure information, which is critical for capturing structural heterogeneity within networks. While CB leverages higher-order cycle information, its inability to account for the diverse and modular nature of real-world networks limits its effectiveness. In contrast, the superior performance of *HOCC* highlights the necessity of combining higher-order cycle attributes with neighborhood interactions and community heterogeneity. This demonstrates that, beyond incorporating higher-order structural information, it is crucial to consider structural heterogeneity to effectively target critical nodes. By integrating higher-order cycles, local interactions, and community structure, *HOCC* achieves a well-balanced and efficient node removal strategy, solidifying its position as a superior algorithm for network disintegration.

4.2.3. Residual network topology

Based on previous observations, DomiRank has proven to be the leading SOTA algorithm across most networks. Therefore, we select the Birmingham and Chicago networks as representative examples to illustrate the resulting network topology after disintegrated by both DomiRank and *HOCC*. As depicted in Fig. 7(a), we compare the disintegration effects of these two algorithms at a specific stage, where the top 10 % of nodes are removed. Under DomiRank, the residual graph sizes in Birmingham and Chicago networks are 9278 and 10,320, respectively. In contrast, the corresponding values under *HOCC* are dramatically lower, with residual sizes of 418 and 529, representing reductions of 95.49 % and 94.87 %, respectively.

Furthermore, we evaluate the final disintegration outcomes, defined by $S(q)$, for both algorithms as demonstrated in Fig. 7(b). Using DomiRank, 28.92 % and 38.09 % of the nodes need to be removed to achieve effective disintegration, resulting in residual networks with 1,220 and 1,190 connected components in Birmingham and Chicago, respectively. Conversely, *HOCC* requires only 25.19 % and 34.99 % of nodes to be removed, yielding more fragmented residual networks with 843 and 675 connected components, respectively.

These findings clearly demonstrate the superior efficiency and effectiveness of *HOCC* in disintegrating infrastructure networks compared to DomiRank. *HOCC* demonstrates a remarkable ability to drastically reduce the size of the residual graph and achieve a higher level of fragmentation with significantly fewer node removals, underscoring its advantages in targeted network disintegration.

4.3. Correlation analysis

As illustrated in Fig. 8, the Grid network serves as an illustrative example to compare node rankings produced by *HOCC* and three classical centrality algorithms: degree, H-index, and betweenness. The critical nodes identified by degree, H-index, and betweenness are densely clustered in specific regions, reflecting the “rich-club” phenomenon, where high-centrality nodes tend to form tightly interconnected hubs. Nodes in close proximity often share overlapping neighborhoods, leading to redundant coverage and reducing the collective impact of their removal on network disintegration.

In contrast, *HOCC* identifies nodes that are more evenly distributed across the network with sparser connections among them. This dispersion minimizes overlap in influence, enabling *HOCC* to effectively disintegrate the network by targeting structurally diverse and globally critical nodes. These results highlight the distinct advantage of *HOCC* in leveraging higher-order structures and community interactions, offering a more effective algorithm compared to traditional centrality algorithms.

To further elucidate the distinctions between *HOCC* and SOTA strategies, Kendall's Tau (τ) is employed to assess the rank correlation across various empirical networks, as illustrated in Fig. 9. The inclusion of Kendall's Tau provides a quantitative comparison of the rankings, transitioning from the visual analyses in Fig. 8 to a deeper statistical perspective.

The average correlations between *HOCC* and benchmarks are generally low, with most values falling below 0.52. Among the benchmarks, Cycle Basis (CB) exhibits the highest average correlation ($\tau = 0.65$), reflecting its partial reliance on cycle-based structures. This moderate similarity is particularly evident in networks such as Sketch ($\tau = 0.80$) and Grid ($\tau = 0.74$). However, unlike *HOCC*, CB does not account for community structure, limiting its applicability to networks with more complex topologies.

Conversely, MSTDC and Domirank show the lowest average correlations with *HOCC* ($\tau = 0.42$ and $\tau = 0.45$, respectively), highlighting their fundamental departure from the ranking framework of *HOCC*. For instance, in networks such as Birmingham ($\tau = 0.16$ for MSTDC) and London ($\tau = 0.33$ for Domirank), these algorithms demonstrate minimal alignment. Notably, while MSTDC is the most effective benchmark in optimizing f_c, and Domirank performs best in terms of R, the low correlations indicate that *HOCC* captures fundamentally different and more impactful structural information, enabling it to achieve superior disintegration performance.

In sparse, large-scale networks such as Sydney, correlations with *HOCC* are generally low, reflecting its ability to leverage global connectivity and sparse structures to identify critical nodes. For instance, MSTDC achieves $\tau = 0.41$, and Domirank reaches $\tau = 0.56$, indicating the distinctiveness of *HOCC* in such networks. In contrast, smaller, denser networks like Chilean exhibit higher correlations with CB ($\tau = 0.88$) and CI ($\tau = 0.64$), due to the dominance of localized cycles and constrained community structures, which align more closely with these benchmarks.

These findings highlight the ability of *HOCC* to uncover unique insights into network disintegration strategies by leveraging higher-order interactions and integrating structural heterogeneity. The combination of visualized distributions and quantitative correlations underscores the superiority of *HOCC* in identifying critical nodes, offering a perspective beyond the reach of traditional and SOTA benchmarks.

5. Conclusion and discussion

While simplex and simplicial complexes offer valuable insights into higher-order interactions within networks, fully connected higher-order structures are seldom observed in CIS due to their operational and geographic constraints. Moreover, these systems often exhibit strong community structures, where indirect connections are more prevalent. To address these limitations, we leverage higher-order cycle structures and community information to design the Higher-Order Cycle Disintegration Framework that captures both direct and subtle indirect influences. The framework reveals intricate connectivity patterns, enabling more efficient and comprehensive network disintegration.

Through extensive and rigorous ablation studies conducted on both synthetic and empirical networks, we demonstrate the superior performance of our proposed framework. Specifically, the introduced algorithm consistently outperforms state-of-the-art algorithms, achieving performance improvements of up to 63.41 % in R and 23.83 % in f_c. We further validate the efficacy of our algorithm through visualizations comparing the topological changes between our algorithm and the leading algorithm, Domirank, at critical thresholds (removing the top 10 % of nodes and reaching the disintegration threshold), underscoring our algorithm's ability to disintegrate networks both quickly and effectively, especially during the early stages.

Additionally, our exploration of the impact of network structure on cycle-related attributes provide valuable insights into the efficiency of our algorithm's topological characteristics. Specifically, our analysis demonstrates that the nodes identified by our algorithm tend to be more dispersed across the network, with nodes situated far apart. In contrast, traditional algorithms exhibit a “rich-club” effect, where critical nodes are tightly clustered. Empirically, our analysis using Kendall's Tau consistently reveals low correlations (below 0.52) between our algorithm and existing state-of-the-art algorithms, further highlighting the distinctive and superior discriminative power of our framework.

In summary, our work introduces a comprehensive and innovative framework for network disintegration, emphasizing the critical importance of higher-order cycle structures, community dynamics, and indirect connections. Our results serve as a valuable reference for the design of effective strategies to identify vulnerable entities in networks, offering critical insights for targeted protection efforts.

The findings underscore the substantial performance benefits embedded in the integrated consideration of higher-order cycle structures and structural heterogeneity. Moving forward, we aim to extend the applicability of this algorithm to other domains, integrating more advanced higher-order cycle information and considering the effects of spatial embeddings. These enhancements hold the potential to further broaden the scope and impact of our algorithm, particularly in reliability analysis.

CRediT authorship contribution statement

Bitao Dai: Conceptualization, Data curation, Methodology, Software, Visualization, Writing – original draft. **Min Wu:** Visualization. **Longyun Wang:** Writing – review & editing. **Jianhong Mou:** Writing – review & editing. **Chaojun Zhang:** Writing – review & editing. **Shuhui Guo:** Visualization. **Suoyi Tan:** Writing – review & editing. **Xin Lu:** Conceptualization, Funding acquisition, Methodology, Supervision, Writing – review & editing.

Declaration of competing interest

The authors declare that they have no known competing financial interests or personal relationships that could have appeared to influence the work reported in this paper.

Acknowledgements

This work is supported by the National Natural Science Foundation of China (72025405, 72474223, 72421002, 92467302, 72301285, 72401039), the Science and Technology Innovation Program of Hunan Province (2023JJ40685, 2024JJ6069, 2024RC3133), the Humanities and Social Sciences Research project of Ministry of Education of China (24YJC630128) and the National University of Defense Technology Cornerstone Project (JS24-04).

Appendix A. Supplementary data

Supplementary data to this article can be found online at https://doi.org/10.1016/j.chaos.2025.116103.

Data availability

Data will be made available on request.

References

[1] Albert R, Jeong H, Barabási A-L. Error and attack tolerance of complex networks. Nature 2000;406:378–82.
[2] Feng K, Ouyang M, Lin N. Tropical cyclone-blackout-heatwave compound hazard resilience in a changing climate. Nat Commun 2022;13:4421.
[3] Zhong L, Lopez D, Pei S, Gao J. Healthcare system resilience and adaptability to pandemic disruptions in the United States. Nat Med 2024;30:2311–9.
[4] Liu S, Fan C, Cheng K, Wang Y, Cui P, Sun Y, et al. Inductive meta-path learning for schema-complex heterogeneous information networks. IEEE Trans Pattern Anal Mach Intell 2024;46:10196–209.
[5] Kasraei A, Garmabaki AHS, Odelius J, Famurewa SM, Chamkhorami KS, Strandberg G. Climate change impacts assessment on railway infrastructure in urban environments. Sustain Cities Soc 2024;101:105084.
[6] Xu M, Ouyang M, Hong L, Mao Z, Xu X. Resilience-driven repair sequencing decision under uncertainty for critical infrastructure systems. Reliability Engineering & System Safety 2022;221:108378.

[7] Zhang H, Xu M, Ouyang M. A multi-perspective functionality loss assessment of coupled railway and airline systems under extreme events. Reliability Engineering & System Safety 2024;243:109831.
[8] Qu S, She Y, Zhou Q, Verschuur J, Zhao L-T, Liu H, et al. Modeling the dynamic impacts of maritime network blockage on global supply chains. The Innovation 2024;5:100653.
[9] Johansson J, Hassel H, Zio E. Reliability and vulnerability analyses of critical infrastructures: comparing two approaches in the context of power systems. Reliability Engineering & System Safety 2013;120:27–38.
[10] Wu J, Tan S, Liu Z, Tan Y, Lu X. Enhancing structural robustness of scale-free networks by information disturbance. Scientific Reports 2017;7:7559.
[11] Ouyang M. Review on modeling and simulation of interdependent critical infrastructure systems. Reliability Engineering & System Safety 2014;121:43–60.
[12] Wu J, Barahona M, Tan Y-J, Deng H-Z. Spectral measure of structural robustness in complex networks. IEEE Transactions on Systems, Man, and Cybernetics-Part A: Systems and Humans 2011;41:1244–52.
[13] Šarūnienė I, Martišauskas L, Krikštolaitis R, Augutis J, Setola R. Risk assessment of critical infrastructures: a methodology based on criticality of infrastructure elements. Reliability Engineering & System Safety 2024;243:109797.
[14] Sun X, Gollnick V, Wandelt S. Robustness analysis metrics for worldwide airport network: A comprehensive study. Chinese Journal of Aeronautics 2017;30:500–12.
[15] Wang K, Liu J, Tian L, Tan X, Peng G, Qin T, et al. Analyzing vulnerability of optical fiber network considering recoverability. Reliability Engineering & System Safety 2022;221:108308.
[16] Hao Y, Jia L, Zio E, Wang Y, He Z. A network-based approach to improving robustness of a high-speed train by structure adjustment. Reliability Engineering & System Safety 2023;243:109857–68.
[17] Lambiotte R, Rosvall M, Scholtes I. From networks to optimal higher-order models of complex systems. Nat Phys 2019;15:313–20.
[18] Yue X, Liu W, Wang X, Yang J, Lan Y, Zhu Z, et al. Constructing an urban heat network to mitigate the urban heat island effect from a connectivity perspective. Sustain Cities Soc 2024;114:105774.
[19] Artime O, Grassia M, De Domenico M, Gleeson JP, Makse HA, Mangioni G, et al. Robustness and resilience of complex networks. Nature Reviews Physics 2024: 1–18.
[20] Braunstein A, Dall'Asta L, Semerjian G, Zdeborová L. Network dismantling. Proc Natl Acad Sci 2016;113:12368–73.
[21] Ren X-L, Gleinig N, Helbing D, Antulov-Fantulin N. Generalized network dismantling. Proc Natl Acad Sci 2019;116:6554–9.
[22] Lou Y, Wang L, Chen G. Structural robustness of complex networks: a survey of a posteriori measures [feature]. IEEE Circuits and Systems Magazine 2023;23:12–35.
[23] Scagliarini T, Artime O, De Domenico M. Assessing the vulnerability of empirical infrastructure networks to natural catastrophes. Chaos, Solitons & Fractals 2025; 191:115813.
[24] Lordan O, Sallan JM, Simo P, Gonzalez-Prieto D. Robustness of the air transport network. Transportation Research Part E: Logistics and Transportation Review 2014;68:155–63.
[25] Wandelt S, Lin W, Sun X, Zanin M. From random failures to targeted attacks in network dismantling. Reliability Engineering & System Safety 2022;218:108146.
[26] Wandelt S, Sun X, Zhang A. Towards analyzing the robustness of the integrated global transportation network abstraction (IGTNA). Transportation Research Part A: Policy and Practice 2023;178:103838.
[27] Ventresca M, Aleman D. A derandomized approximation algorithm for the critical node detection problem. Computers & Operations Research 2014;43:261–70.
[28] Veremyev A, Boginski V, Pasiliao EL. Exact identification of critical nodes in sparse networks via new compact formulations. Opt Lett 2014;8:1245–59.
[29] Wang Z, Deng Y, Wang Z, Wu J. Disintegrating spatial networks based on region centrality. Chaos: An Interdisciplinary. Journal of Nonlinear Science 2021;31: 061101.
[30] Engsig M, Tejedor A, Moreno Y, Foufoula-Georgiou E, Kasmi C. DomiRank Centrality reveals structural fragility of complex networks via node dominance. Nat Commun 2024;15:56.
[31] Zhang J, Zhou Y, Wang S, Min Q. Critical station identification and robustness analysis of urban rail transit networks based on comprehensive vote-rank algorithm. Chaos, Solitons & Fractals 2024;178:114379.
[32] Mugisha S, Zhou H-J. Identifying optimal targets of network attack by belief propagation. Physical Review E 2016;94:012305.
[33] Clusella P, Grassberger P, Pérez-Reche FJ, Politi A. Immunization and targeted destruction of networks using explosive percolation. Phys Rev Lett 2016;117: 208301.
[34] Wang S, Liu J. Constructing robust community structure against edge-based attacks. IEEE Systems Journal 2019;13:582–92.
[35] Deng Y, Wu J, Xiao Y, Zhang M, Yu Y, Zhang Y. Optimal disintegration strategy with heterogeneous costs in complex networks. IEEE Trans Syst Man Cybern Syst 2018;50:2905–13.
[36] Fan C, Zeng L, Sun Y, Liu Y-Y. Finding key players in complex networks through deep reinforcement learning. Nature Machine Intelligence 2020;2:317–24.
[37] Grassia M, De Domenico M, Mangioni G. Machine learning dismantling and early-warning signals of disintegration in complex systems. Nat Commun 2021;12:5190.
[38] Morone F, Makse HA. Influence maximization in complex networks through optimal percolation. Nature 2015;524:65–8.
[39] Wandelt S, Shi X, Sun X. Estimation and improvement of transportation network robustness by exploiting communities. Reliability Engineering & System Safety 2021;206:107307.
[40] Xu M, Pan Q, Muscoloni A, Xia H, Cannistraci CV. Modular gateway-ness connectivity and structural core organization in maritime network science. Nat Commun 2020;11:2849.
[41] Dai B, Mou J, Tan S, Cai M, Liljeros F, Lu X. The role of link redundancy and structural heterogeneity in network disintegration. Expert Systems with Applications 2024;255:124590.
[42] Hong L, Zhong X, Ouyang M, Tian H, He X. Vulnerability analysis of public transit systems from the perspective of urban residential communities. Reliability Engineering & System Safety 2019;189:143–56.
[43] Dai B, Qin S, Tan S, Liu C, Mou J, Deng H, et al. Identifying influential nodes by leveraging redundant ties. J Comput Sci 2023;69:102030.
[44] Requião da Cunha B, González-Avella JC, Gonçalves S. Fast fragmentation of networks using module-based attacks. PloS One 2015;10:e0142824.
[45] Cong W, Hu M, Dong B, Wang Y, Feng C. Empirical analysis of airport network and critical airports. Chin J Aeronaut 2016;29:512–9.
[46] Battiston F, Amico E, Barrat A, Bianconi G, Ferraz de Arruda G, Franceschiello B, et al. The physics of higher-order interactions in complex systems. Nat Phys 2021; 17:1093–8.
[47] Benson AR, Gleich DF, Leskovec J. Higher-order organization of complex networks. Science 2016;353:163–6.
[48] Battiston F, Cencetti G, Iacopini I, Latora V, Lucas M, Patania A, et al. Networks beyond pairwise interactions: structure and dynamics. Phys Rep 2020;874:1–92.
[49] Fang F, Ma J, Ma Y-J, Boccaletti S. Social contagion on higher-order networks: the effect of relationship strengths. Chaos, Solitons & Fractals 2024;186:115149.
[50] Shi D, Chen G. Simplicial networks: a powerful tool for characterizing higher-order interactions. Natl Sci Rev 2022;9:nwac038.
[51] Shi D, Lü L, Chen G. Totally homogeneous networks. Natl Sci Rev 2019;6:962–9.
[52] Shi D, Chen Z, Sun X, Chen Q, Ma C, Lou Y, et al. Computing cliques and cavities in networks. Communications Physics 2021;4:249.
[53] Fan T, Lü L, Shi D, Zhou T. Characterizing cycle structure in complex networks. Communications Physics 2021;4:272.
[54] Shi W, Xu S, Fan T, Lü L. Cost effective approach to identify multiple influential spreaders based on the cycle structure in networks. Science China Information Sciences 2023;66:192203.
[55] Zhao Y, Li C, Shi D, Chen G, Li X. Ranking cliques in higher-order complex networks. Chaos: An Interdisciplinary Journal of Nonlinear Science 2023:33.
[56] Schneider CM, Moreira AA, Andrade Jr JS, Havlin S, Herrmann HJ. Mitigation of malicious attacks on networks. Proc Natl Acad Sci 2011;108:3838–41.
[57] Blondel VD, Guillaume J-L, Lambiotte R, Lefebvre E. Fast unfolding of communities in large networks. Journal of Statistical Mechanics: Theory and Experiment 2008; 2008:P10008.
[58] Lancichinetti A, Fortunato S, Radicchi F. Benchmark graphs for testing community detection algorithms. Physical Review E 2008;78:046110.
[59] Wang Z, Deng Y, Dong Y, Kurths J, Wu J. Spatial network disintegration based on ranking aggregation. Inf Process Manag 2025;62:103955.
[60] Kunegis J. Konect: the koblenz network collection. Proceedings of the 22nd International Conference on World Wide Web2013. p. 1343–50.
[61] Rossi R, Ahmed N. The network data repository with interactive graph analytics and visualization. In: Proceedings of the AAAI Conference on Artificial Intelligence; 2015.
[62] Chen D-B, Gao H, Lü L, Zhou T. Identifying influential nodes in large-scale directed networks: the role of clustering. PloS One 2013;8:e77455.
[63] Xu X, Zhu C, Wang Q, Zhu X, Zhou Y. Identifying vital nodes in complex networks by adjacency information entropy. Sci Rep 2020;10:1–12.
[64] Freeman LC. A set of measures of centrality based on betweenness. Sociometry 1977:35–41.
[65] Huang Y, Wang H, Ren X-L, Lü L. Identifying key players in complex networks via network entanglement. Communications Physics 2024;7:19.
[66] Kendall MG. A new measure of rank correlation. Biometrika 1938;30:81–93.